Noninvasive Measurements and Analysis of Blood Velocity Profiles in Human Retinal Vessels

Zhangyi Zhong, Hongxin Song, Toco Yuen Ping Chui, Benno L. Petrig, and Stephen A. Burns

Purpose. To quantitatively model the changes in blood velocity profiles for different cardiac phases in human retinal vessels.

Methods. An adaptive optics scanning laser ophthalmoscope (AOSLO) was used to measure blood velocity profiles in three healthy subjects. Blood velocity was measured by tracking erythrocytes moving across a scanning line. From the radial position of the cells within the lumen, the blood velocity profile was computed. The cardiac pulsatility was recorded with a cardiac signal monitor.

Results. The shape of the blood velocity profile in retinal arteries changed systematically during the cardiac cycle, with the flattest profile occurring during the diastolic phase. The measured blood velocity profiles were typically flatter than the commonly assumed parabolic shape. The flatness increased with decreasing vessel size. For the large veins (>80 μm), the ratio of the centerline velocity to the cross-sectional average velocity was between 1.50 and 1.65. This ratio decreased to 1.36 in the smallest vein studied (32 μm). Velocity profiles downstream from a venous confluence showed two peaks at 120 μm from the confluence, but a single velocity peak 500 μm downstream from the confluence.

Conclusions. The cardiac cycle influences the blood flow velocity profiles systematically in retinal arteries but not in veins. Parabolic flow was not found in even the largest vessels studied, and deviations from parabolic flow increased in smaller vessels. The measurements are sensitive enough to measure the dual-humped blood velocity profile at a vein confluence. (*Invest Ophthalmol Vis Sci.* 2011;52:4151–4157) DOI:10.1167/iovs.10-6940

Sufficient blood flow in retinal vessels is essential for maintaining healthy retinal tissues, because the delivery of nutrients and removal of waste depend on the volumetric flow rate of blood, which is determined not only by the centerline velocity and size of the vessels, but also by the shape of the blood velocity profile across the vessel lumen. Understanding how the profile varies with vessel size and cardiac cycle will thus improve the calculation of the cross-sectional average blood velocity and the total flow rate. Furthermore, measurements of blood velocity near the vessel wall can provide useful information about shear stress at the vessel wall, which is related to endothelial cell shape[1] and function.[2] It has been reported that atherosclerotic lesions tend to originate in areas of disturbed flow associated with low wall-shear stress.[3] There are also important reasons to understand how flow is affected by retinal disorders,[4] such as diabetic retinopathy[5–8] and glaucoma.[9–11]

While fluid mechanics suggest that an ideal fluid should have a parabolic velocity profile, the actual distribution of blood velocity across a blood vessel is not well understood. Parabolic blood velocity profiles can be obtained in large glass tubes.[12,13] However, some in vivo studies suggest that the blood velocity profile is blunter than is predicted by a parabolic shape.[14–16] Logean et al.[17] found that blood velocity profiles during the diastolic and systolic phases are not significantly different from the parabolic shape in vessels with a diameter larger than 100 μm, although all the vessels measured tended to present some degree of profile blunting.

If the blood velocity profile in vessels deviates from a parabolic shape, physical considerations suggest that the shape should be velocity dependent.[18] In the human retina, researchers have measured blood velocity profiles by optical coherence tomography, but they fit their data assuming a parabolic flow, rather than using their data to model the actual blood velocity variation.[19,20] Since the shape of the blood velocity profile in retinal arteries could change due to cardiac pulsatility,[14] it is important to assess multiple instantaneous velocity profiles at different cardiac phases in retinal arteries, not just the systolic and diastolic phases.

In the present study we used an adaptive optics scanning laser ophthalmoscope (AOSLO) to make precise, time-resolved measurements of blood velocity profiles in retinal veins and arteries. The AOSLO makes this possible by providing in vivo retinal images with near-diffraction–limited lateral resolution.[21–25] Because this technique is based on direct imaging of the light backscattered by erythrocytes, it does not require injection of any contrast dye. The blood velocity profiles were measured in retinal blood vessels of a wide range of lumen sizes. The ratio of the centerline velocity to the cross-sectional average velocity in retinal veins was fitted as a function of vessel size.

Methods

AOSLO Imaging System

Blood velocity measurements are obtained using the Indiana AOSLO system described by Ferguson et al.[26]. In brief, a supercontinuum laser (Fianium, Beverly, MA) with an 840-nm filter (12-nm bandwidth) was used as the imaging source. Wavefront errors were detected with a Shack-Hartmann sensor. Two deformable mirrors were used to correct different orders of optical aberrations of the eye, to obtain near-diffraction–limited imaging resolution.[27] The spatial resolution of the AOSLO system is 2.5 μm for a dilated pupil (7 mm typically).

The laser beam scan was performed with a 10-kHz line scanner and a programmable vertical scanner. To increase the sampling rate, both

From the School of Optometry, Indiana University, Bloomington, Indiana.

Supported by National Institutes of Health Grants EY14375, EY04395, and P30EY019008.

Submitted for publication November 23, 2010; revised January 24 and February 14, 2011; accepted March 28, 2011.

Disclosure: **Z. Zhong**, None; **H. Song**, None; **T.Y.P. Chui**, None; **B.L. Petrig**, None; **S.A. Burns**, None

Corresponding author: Stephen A. Burns, Indiana University, School of Optometry, 800 East Atwater Avenue, Bloomington, IN 47405-3635; staburns@indiana.edu.

directions of each line scan were captured and treated as two separate lines by the frame grabber. The time interval is constant in the center of the scan and becomes uneven toward the scan edges. However, the average time interval across the entire scan remains constant, producing a scan frequency of 20 kHz. All blood velocity measurements in this study used >15 lines for image processing, which smoothed out the influence of local time interval unevenness. What's more, the measurements were obtained within the central 20% range of the scan where the interval unevenness is at a minimum.

The subject's head movements were minimized with a chin rest. A 30° imaging system (Physical Sciences Inc., Andover, MA) provided a simultaneous en face image, and the high-resolution AOSLO image could be directed to any region within the wide field image by displacing the beam under computer control.[28]

Human Subjects

Three subjects were tested. Informed consent was obtained from the subjects after explanation of the nature and possible consequences of the study. The eyes were dilated with 0.5% tropicamide. When the vertical scan was running, the exposure to the imaging beam (200 μW, 840 nm) and the wavefront-sensing beacon (50 μW, 740 nm) were more than 10 times below the ANSI safe exposure level for continuous viewing at this field size (780 × 540 μm). When the vertical scan was stopped, the same optical power was spread on a smaller field size (according to the calculations for the standard, 780 × 25 μm), but the exposure was still safe according to ANSI standards. The vertical scan motion was programmed to resume every frame (it was never stationary for longer than 30 ms), which ensured safety and comfort. The research protocol of in vivo imaging of human retinal blood flow described in this article and the consent form were approved by the Indiana University Institutional Review Board (Ethics Committee) and met the requirements of the Declaration of Helsinki.

Erythrocyte Movement Tracing and Velocity Calculation

To use the AOSLO for measuring blood cell velocities, we implemented a line scan mode, in which the vertical scan was programmed to pause briefly during each frame.[29] Pausing the vertical scan on top of the target blood vessel enabled the line scan to repeatedly scan across it, allowing 20-kHz sampling of the same intersectional area. During this pause, the partial image frame formed by the frame grabber consists of a direct measure of the intensity change over time for each pixel of the scan line intersecting the vessel at a narrow angle. The horizontal position in this partial image thus represents the position along the scan direction, and the vertical dimension represents time. We therefore refer to this partial image as the XT image. As an erythrocyte passes through the scanned area, it introduces intensity changes. Because the line scans are obtained rapidly, the movement of the erythrocyte produces a diagonal streak spanning several lines in the XT image. Different erythrocytes will form different diagonal streaks. The slope of the diagonal streak represents the erythrocyte velocity in the scan direction, given the time interval between line scans (Fig. 1). An offline image-processing program in commercial software (MatLab; The MathWorks, Natick, MA) was used to measure these slopes. Typically, the time (related to the number of selected image lines in the XT image) required for a single velocity measurement was less than 3 ms. This high sampling frequency minimizes the influence of eye movements. Moreover, during the XT portion of each frame, we can detect the motion of the eye based on the fact that stationary structures should appear as vertical straight lines (Fig. 1). If there is a horizontal eye movement, then these lines will deviate from the vertical. If there is a vertical component of motion and the stationary structures are small, then the scan line will be moved off the structure, and the vertical lines will be interrupted. We restricted our data analysis to measurements taken in images with clean, straight, vertical lines and minimal interframe motion.

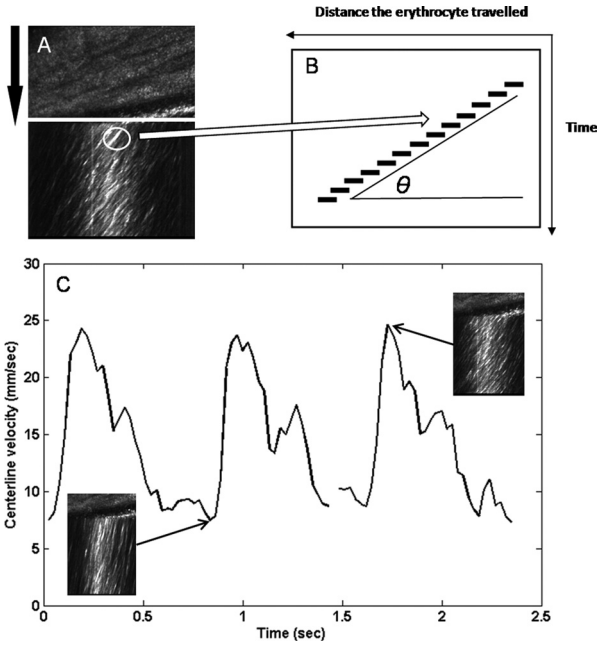

FIGURE 1. (**A**) XT image with erythrocyte motion trails appearing as bright streaks. The partial frame below the horizontal scanning line (*horizontal line*) is the XT image. The crossing angle α between the scanning line and the vessel axis was 15°. (**B**) A schematic diagram of one of the erythrocyte motion trails. The horizontal axis is the distance the erythrocyte traveled in the direction of the scan line; the vertical axis plots time increasing downwards. The steeper the slope, the slower the erythrocyte moves. (**C**) The centerline blood velocity in an 82-μm retinal artery fluctuated with the heartbeat (subject 2, 27 years old). One of AOSLO XT images was excluded because of eye motion. The XT images at one of the systolic phases and one of the diastolic phases were included. The blood velocity fluctuation is reflected by the slope changes of the erythrocyte motion trails across cardiac cycles.

Based on the slope angle θ ($0 < \theta < \pi/2$) of the streaks in the XT image, V_p, the component of erythrocyte velocity in the scan direction, can be calculated:

$$V_p = \frac{f \cdot \cot\theta}{k} \quad (1)$$

where f is the horizontal scan frequency (20 kHz), and k is the system magnification calculated taking into account the axial length of the subject's eye.[23] V_p is then adjusted by the angle α between the scanning line and the vessel axis, to compute the erythrocyte velocity V_{ax} along the axis of the blood vessel:

$$V_{ax} = \frac{V_p}{\cos\alpha} \quad (2)$$

Because the blood vessel and its surrounding tissue interacted with the light differently, two vertical straight intensity gaps formed at the edges of the vessel in the XT image. The intensity gaps were used to calculate the vessel diameter by taking into account the angle α.

Blood Velocity Profile Measurements

Human erythrocytes at rest have a biconcave shape, with a diameter of approximately 8 μm and a thickness of approximately 2 μm.[30] Erythrocytes flowing in blood vessels deform due to flow shear stress.[31] The deformed erythrocytes resembled prolate ellipsoids with a width of 4 to 5 μm based on our AOSLO images, similar to results reported in other studies.[31,32] Thus, to measure the blood velocity profile, we

divided the intersectional area of our scanning beam with the blood vessel into multiple equal-width (5-μm) columns, which represent lumen samples at different radial positions.

The blood velocity profile measurements are based on the assessment of the velocities of erythrocytes moving in multiple files in the central plane of the blood vessel. However, the depth of focus of the AOSLO system is still relatively large. For the 100-μm diameter confocal aperture we used (2.01 times the airy disc diameter), the depth of focus is approximately 110 μm.[12,33] As a result, the images include scattered light coming from the red blood cells (RBCs) moving above or below the primary focal plane. To further improve accuracy, for each sample column in the XT image, the velocity of the fastest-moving particle (the shallowest slope) is assumed to represent the blood velocity for the central plane inside the sample volume, since particles at the central plane move at the highest speed (a result supported by our measurements of the radial velocity distribution). Calculating the blood velocity in each column enabled us to measure the blood velocity profile at the central plane across the lumen. Regardless of the orientation of the vessel to be measured, a rotatable stage allowed the alignment of the scan line to cross the blood vessel at a small angle, increasing the width and spatial resolution of the intersection area in the XT image, where we measured the blood velocity profile. The sampling rate of our blood velocity profile measurement (the frame rate) was 37 Hz, which is sufficient to track the influence of cardiac pulsatility on profile shapes (i.e., 30 profiles per heart beat for a resting heart rate of 75 beats per minute).

Blood Velocity Measurement Synchronization with Cardiac Cycle

A photoplethysmograph was attached to the subject's earlobe to record the cardiac pulse waveform synchronously with the AOSLO video frames. The output signal of the photoplethysmograph was digitized and saved, along with each AOSLO image into a data file. Therefore, the corresponding cardiac phase of each instantaneous blood velocity profile measurement was known, allowing us to group profile measurements from the same cardiac phase in multiple cycles.

Blood Velocity Profile Modeling

In retinal vessels larger than 30 μm, the erythrocytes flow in multiple lanes and tend to concentrate in the central core region, generating a cell-depleted region near the vessel wall. Secomb[34] determined that this cell-depleted region (plasma layer) was approximately 1.8 μm thick, providing a close fit to the empiric curve for microvessels with lumen diameters ranging from 30 to 1000 μm. As a result, for techniques based on cell tracing, few velocity data can be obtained within 1.8 μm of the vessel wall. In studies on blood velocity profiles in large blood vessels (lumen size, >100 μm), investigators often assumed that the blood velocity at the vessel wall was 0 in their models of the velocity distribution across the lumen.[17,19,35] In large blood vessels, the influence of this approximation is negligible because the blood velocity profile in a large vessel has many measurements and is thus robust to outliers. However, in the medium and smaller retinal vessels (lumen size, <100 μm) reported in this study, forcing the velocity to be 0 at the vessel wall caused large errors in the fits at the center. We therefore chose not to force the blood velocity at the vessel wall to be 0; rather, we fitted only our directly measured data points. More details on this rationale are presented in the Discussion section.

Assuming an axially symmetric velocity profile, we can express the blood velocity profile on the central plane of a straight blood vessel as

$$V(r) = V_{max}\left[1 - (1 - \beta)\cdot\left|\frac{r}{R}\right|^{B}\right],\ (0 \le |r| \le R,\ 0 \le \beta \le 1) \quad (3)$$

where $V(r)$ is the velocity at radial position r, V_{max} is the centerline velocity, R is the radius of the blood vessel cross section, and B is a bluntness index. The parameter β is a scale factor that models the extrapolated speed at the edge of the vessel, ignoring the cell-free layer. Both the bluntness index B and the scale factor β contribute to the flatness of the blood velocity profile. To compare the shape of different blood velocity profiles, we normalized the blood velocity profiles to their centerline velocities V_{max} (Fig. 2). We calculated the average velocity ($V_{average}$) based on the total volume of blood by rotating the blood velocity profile around the vessel axis and calculating the average over the whole cross-sectional lumen area.

The velocity ratio η between the centerline velocity V_{max} and the cross-sectional average velocity $V_{average}$ from equation 3 defines the flatness of the blood velocity profile. The smaller the velocity ratio, the flatter the velocity profile. The velocity ratio of the assumed axially symmetric blood velocity profile can be approximated by

$$\eta = \frac{V_{max}}{V_{average}} = \frac{B + 2}{B + 2\cdot\beta}. \quad (4)$$

Thus, the average velocity is influenced by both the bluntness index B and the scale factor β.

Results

Blood Velocity Profiles in Straight Retinal Arteries

Ninety blood velocity profiles in a straight retinal artery (72 μm) of subject 2 (27 years old) were measured for three cardiac cycles occurring within 2.28 seconds. The centerline velocity fluctuated three times in the 2.28 seconds, matching closely the subject's heart rate, as recorded by the photoplethysmography data. For each velocity profile, the measured centerline velocity V_{max} was then normalized into the range of [0,1] (V_{norm}) using the systolic centerline velocity $V_{systolic}$ and the diastolic centerline velocity $V_{diastolic}$:

$$V_{norm} = \frac{V_{max} - V_{diastolic}}{V_{systolic} - V_{diastolic}}. \quad (5)$$

Based on the normalized centerline velocity, V_{norm}, the profile measurements were grouped into five velocity divisions with equal spacing (i.e., 0.2 spacing in the normalized range of [0,1] during the cardiac cycle). The centerline velocity in division 1 was the lowest (diastolic cardiac phase) and that in division 5

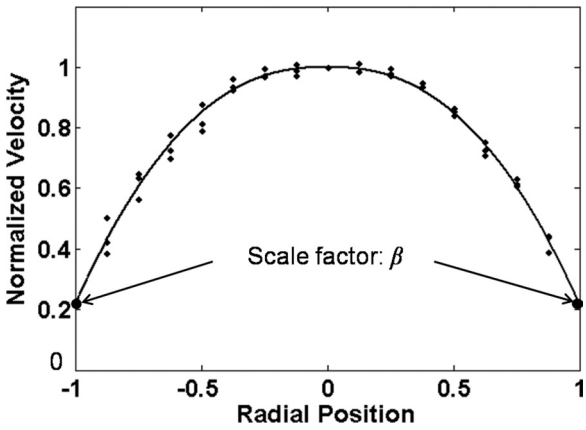

Figure 2. An example of the normalized blood velocity profile data and the fit of equation 3 to the data. The *x*-axis is the normalized radial position. The extrapolated speed at the edges of the vessel is annotated as the two *large filled circles*. Since the blood velocity profile is assumed to be symmetric, the extrapolated speed at both edges is the same, as modeled by the scale factor β. Data for three repeat measurements are plotted as separate points.

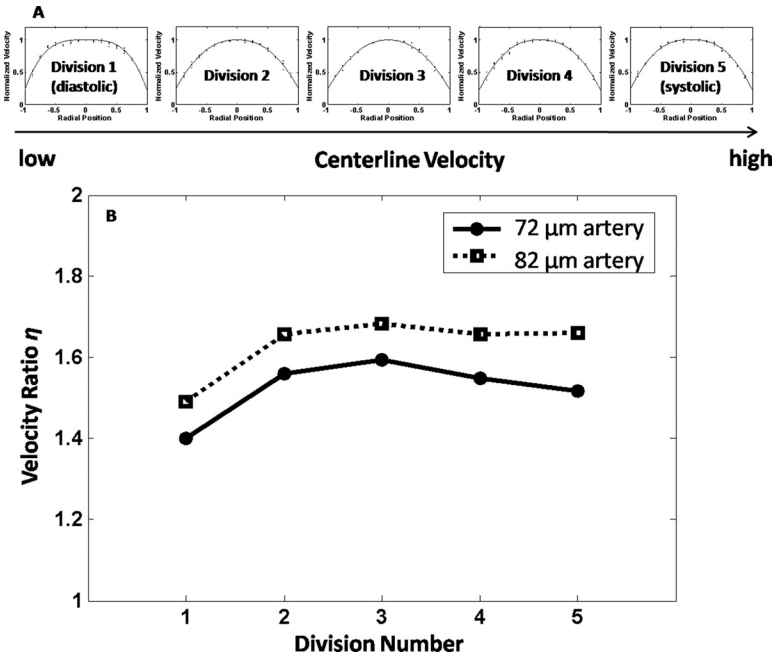

FIGURE 3. (**A**) Fitted normalized blood velocity profile shapes for a 72-μm artery. (**B**) Velocity ratio η for different velocity divisions of the two studied arteries.

was the highest (systolic cardiac phase). The velocity profiles were then renormalized to their centerline velocities V_{max}. For each division, three instantaneous normalized blood velocity profiles were fitted according to equation 3, using a curve fitting tool box (MatLab; The MathWorks). The same analysis was applied to profile measurements of another straight retinal artery (82 μm) of the same subject. The velocity ratios η in the five divisions for both arteries are shown in Figure 3, together with the fitted profiles for the 72-μm artery. The fitting parameters for both arteries are shown in Table 1.

The shape of the blood velocity profiles in the target arteries changed across cardiac phases, agreeing with the results found by Nakano et al.[14] Among the five velocity divisions, the blood velocity profile of division 1 (diastolic cardiac phase) was the flattest, associated with the smallest velocity ratio. In all cardiac phases, the fitted blood velocity profiles in the target retinal artery were flatter than that predicted by parabolic flow, with the velocity ratio lower than 2 in all our observations.

Blood Velocity Profiles in Straight Retinal Veins

Blood velocity profiles were measured in retinal veins of different lumen sizes. For each vein, three instantaneous normalized blood velocity profiles were used for curve fitting according to equation 3. No significant differences in velocity profiles were found across cardiac phases for the same retinal vein. Table 2 lists the fitting parameters.

We did not measure the velocity ratio in retinal vessels smaller than 30 μm. However, Yen et al.,[36] using a larger scale model, reported a value of 1.19 for the velocity ratio in 8-μm capillaries. By assuming a velocity ratio of 2 for an infinitely large vessel and including 1.19 as the velocity ratio for 8-μm capillaries, a descriptive function of the velocity ratio in terms of vein diameter D was fit on the basis of the data in Table 2 (Fig. 4):

$$\eta = 2 \cdot (1 - 0.5428 \cdot e^{-\sqrt{0.0087 \cdot D}}). \quad (6)$$

The R^2 for the fit is 0.937.

Blood Velocity Profile at a Venous Confluence

Figure 5 shows velocity profile measurements downstream of a venous confluence in subject 2. Here, the velocity profile differed significantly from those measured in straight vessels. The blood velocity profile near the venous confluence was not symmetric and thus could not be fitted by equation 3. This phenomenon indicates that the two blood flow streams from the two merging veins did not merge immediately, but rather displayed the flow characteristics of the two separate parent veins. The peaks of the two blood velocity subprofiles, especially those coming from the larger vein, were skewed toward the center of the two streams, indicating a higher shear rate. Further downstream from the venous confluence, the blood velocity profile merged and eventually showed the expected symmetric radial distribution. The observed blood velocity profile disruption and recovery agree with the measurements reported by Logean et al.[17] using confocal laser Doppler velocimetry.

TABLE 1. Fitting Parameters of the Blood Profiles for the Data in Figure 3

	Division 1	Division 2	Division 3	Division 4	Division 5
72-μm artery					
Bluntness index B	3.40	2.34	2.13	2.40	2.58
Scale factor β	0.23	0.22	0.23	0.22	0.22
82-μm artery					
Bluntness index B	2.64	2.01	1.79	1.85	1.94
Scale factor β	0.24	0.21	0.23	0.24	0.22

TABLE 2. The Parameters of the Blood Profiles for Different Size Retinal Veins

Vein Diameter D (μm)	Bluntness Index B	Scale Factor β	Velocity Ratio η
107	2.57	0.10	1.65
101	2.62	0.13	1.60
96	2.44	0.20	1.57
92	2.41	0.25	1.52
82	2.57	0.20	1.54
75	2.65	0.24	1.49
73	2.64	0.22	1.51
61	2.66	0.24	1.48
59	2.73	0.22	1.49
49	2.57	0.35	1.40
46	2.35	0.40	1.38
32	2.23	0.44	1.36

DISCUSSION

The blood velocity profile–fitting model described in equation 3 differs from the commonly used blood velocity profile equation

$$V(r) = V_{max}\left(1 - \left|\frac{r}{R}\right|^{K}\right),\ (0 \le |r| \le R) \qquad (7)$$

where $V(r)$ is the velocity at radial position r, V_{max} is the centerline velocity, and R is the radius of the blood vessel cross section, K is the bluntness index without any scale factor involved.[17,18] Equation 7 forces the velocity at the wall to be 0, according to the nonslip boundary condition.[37] Because equation 7 does not include a scale factor β, the bluntness index K works differently from our bluntness index B, defined in equation 3, in describing the flatness of the blood velocity profile. Although the model of equation 7 worked for our larger vessels (lumen size, >100 μm) as reported by others,[17,19,35] there were systematic fitting errors for medium or smaller vessels, including systematic underestimation of velocities near the vessel wall and overestimation of velocities near the lumen center. Figure 6 presents an example with a 72-μm artery. The dashed curve in Figure 6A is the best fit for equation 7 and the solid curve for equation 3, together with the residual errors in Figure 6B. Fitting according to equation 3 (solid curve) generates significantly smaller mean residuals than does equation 7 ($P = 0.0012$ for a one-tailed t-test with 95% CI). Equation 3 therefore fits both small and large vessel velocity profiles, since for the large vessels the scale factor β is small (Table 1). When the scale factor is 0, equation 3 becomes mathematically equivalent to equation 7. However, for medium or smaller blood vessels, equation 3 offers a more accurate model of the blood velocity profile (Fig. 6).

The success of fitting by equation 3 does not imply that the nonslip boundary condition[37] is incorrect. We are fitting the velocity distribution in the central core of the lumen, and because the plasma layer has no information on the vessel-wall–limiting condition. With no cells present the fluid viscosity of the near-wall region is presumably different from the rest of the lumen. As a result, the velocity distribution in the near-wall region should be modeled separately to satisfy the nonslip condition, especially in medium-sized or smaller vessels and not be modeled across the entire lumen as equation 7 does. Tangelder et al.[38] have proposed a linear decline model for the blood velocity distribution in the near-wall region,[38] which will fulfill the nonslip boundary condition. Our fitting model for the central core region, along with the linear decline model in the near-wall region, can constitute a two-tiered modeling method that may provide a better theoretical description of the velocity distribution across the whole lumen. However, for calculating the average cross-sectional velocity, using our fitting method described in equation 3 across the whole lumen does not introduce a large error, because the volume of blood in the near-wall region is small compared with the central volume. Even for the smallest vessel we studied (32 μm), the error is less than 5%, and the error is smaller in larger vessels.

In contrast, for calculation of wall shear, the nature of the velocity variation in the cell-poor layer near the vessel wall is important and necessitates separate modeling. The present model helps establish the boundary condition for the velocities at the interface between the near-wall region and central core of the blood vessel, which is essential for the linear decline modeling in the near-wall region.

The concept of scale factor β was first introduced by Tangelder et al.[15] to address the problem described in Figure 6. By assuming a symmetric blood velocity profile, their method of fitting can be expressed as:

$$V(r) = V_{max}\left(1 - \left|\beta \cdot \frac{r}{R}\right|^{B}\right),\ (0 \le |r| \le R, 0 \le \beta \le 1). \qquad (8)$$

They originally introduced β as a mathematical parameter with no physical meaning. We slightly modified their model, to link the scale factor β directly to the intercept value of the fitting curve against the vessel wall, as described in equation 3. In this way, the scale factor can directly describe how much the velocity decreases from the centerline to the near-wall region, in other words, how "flat" the blood velocity profile is. When it comes to small retinal blood vessels, the scale factor plays an increasingly important role in influencing the flatness of blood velocity profile. The data in Table 2 show that for veins smaller than 50 μm, although the bluntness index B decreases, the scale factor β increases markedly with decreasing lumen size. Influenced by the two parameters, the velocity ratio η decreases with the lumen size, which indicates that the blood velocity profile gets flatter when the lumen size decreases, as reported by Gaehtgens et al.[39]

Our calculated velocity ratio, the profile flatness indicator, differs from the empiric velocity ratio introduced by

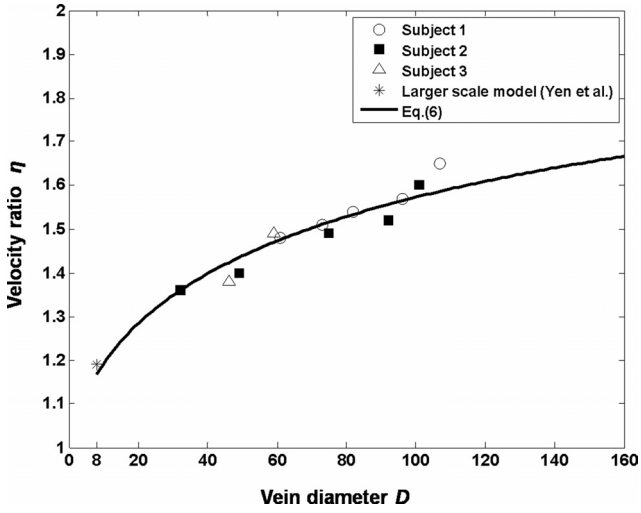

FIGURE 4. Scatterplot of the data together with the fit according to equation 6. The star symbol indicates the ratio for 8 μm capillaries from a larger scale model.

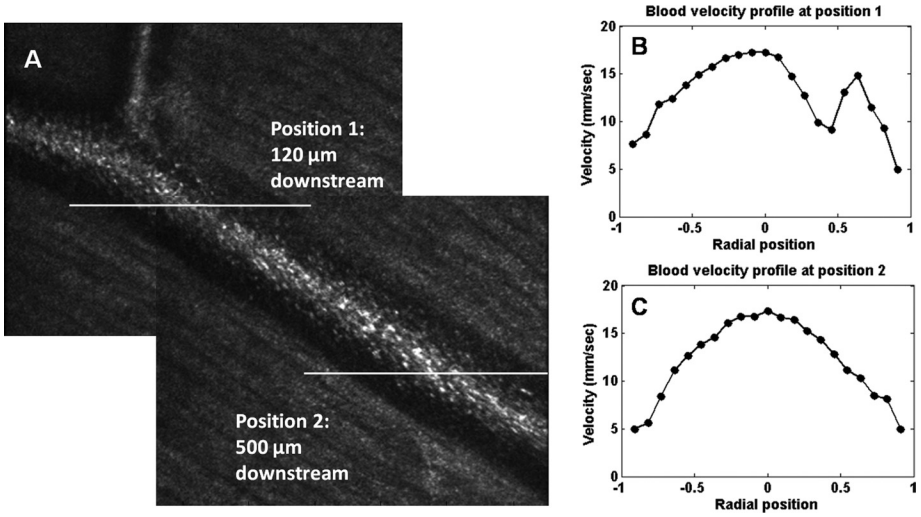

FIGURE 5. Blood velocity profiles for a median cardiac phase at different locations downstream of a vein confluence. (**A**) The high-resolution AOSLO image at the target vein confluence (115 μm). *Horizontal lines*: the scanning line positions. (**B**) The blood velocity profile at position 1 (120 μm downstream). The two peaks from the original confluent streams can be clearly seen. (**C**) The blood velocity profile at position 2 (500 μm downstream). The profile shape appears more regular than that in (**B**).

Baker et al.[40] The purpose of their velocity ratio is to adjust for the signal averaging artifact in double-slit photometric measurements. Their ratio of 1.6 is actually for Poiseuille flow, with a parabolic profile, and does not suggest flatter profiles. Our data are consistently flatter than predicted by Poiseuille flow suggesting that Poiseuille (laminar) flow does not apply in retinal blood vessels, although the deviation from parabolic profiles is smaller in large retinal vessels than in smaller retinal vessels. In retinal arteries, the blood velocity profile of at the diastolic cardiac phase is the flattest, which may result from more erythrocyte aggregation when the centerline velocity decreases, as reported by Bishop et al.[18] The velocity ratio function described in equation 6 cannot directly apply to retinal arteries, because it does not consider the influence of cardiac pulsatility on velocity profile flatness.

We determined the blood velocity in blood vessels as small as 32 μm. For even smaller vessels the concept of a profile becomes difficult. Although we can measure velocity in these smaller vessels, individual blood cells occupy a significant proportion of the lumen and other constraints emerge for describing blood velocity including cell–cell interactions.

For the current system the line scan frequency is 20 kHz. This scan frequency represents a fundamental sampling rate for this technique, just as it does for the similar approach used by the Heidelberg flowmeter (Heidelberg Engineering Heidelberg, Germany),[41] although the line scan frequencies for the two techniques are different. Directly related to this fundamental sampling rate, the upper limit of the measurable blood velocities for the current system is approximately 100 mm/s. However, this upper limit is only for the velocity components in the direction of the scanning line—in other words, the V_p described in equation 2. Since we can rotate our line scan to adjust the angle α between the scanning line and the vessel axis, the upper limit in our system is adequate for even the largest retinal arteries. Another simpler solution for improving the upper limit is to install a faster line scanner, which will help more directly in facilitating high-velocity profile measurements.

If the target blood vessel were oriented at an angle in depth, we would underestimate the absolute velocity. However, since the underestimation will apply to all data points in a blood velocity profile, this underestimation factor will be eliminated after the velocity measurements are normalized against the profile centerline velocity. For our data, the underestimation was small, because most of the vessels in the size range of interest lay approximately in the plane of the retina,[42] and we chose regions where the vessels remained in good focus over a considerable lateral extent.

CONCLUSION

The blood velocity measurements in retinal arteries corresponded well with the cardiac cycle. The bluntness of the blood velocity profile changed across the cardiac cycle in retinal arteries, but not in veins. In retinal arteries, the blood velocity profiles were bluntest at the minimum centerline velocity phase. The ratio η between the centerline velocity V_{max} and the cross-sectional average blood velocity $V_{average}$ decreased with decreasing lumen size in retinal veins and was lower than 2 for all the retinal vessels. Immediately after the vein confluence, the blood velocity profile had an asymmetric shape with two peaks, because the flows from branch veins were not fully merged. The blood velocity profile developed into the expected symmetric single-peak shape further downstream from the vessel junction. The AOSLO can measure

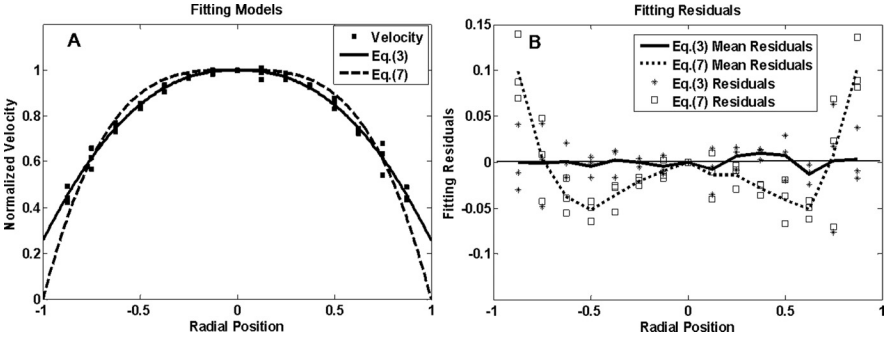

FIGURE 6. Comparison between fitting models to an instantaneous blood velocity profile measured in a medium-sized retinal artery (72 μm).

blood velocity profiles in retinal blood vessels of a wide size range, providing unprecedented accuracy and resolution of retinal blood flow measurements, both spatially and temporally.

References

1. Sato M, Ohshima N. Flow-induced changes in shape and cytoskeletal structure of vascular endothelial-cells. *Biorheology.* 1994;31:143–153.
2. Gnasso A, Carallo C, Irace C, et al. Association between wall shear stress and flow-mediated vasodilation in healthy men. *Atherosclerosis.* 2001;156:171–176.
3. Zarins CK, Giddens DP, Bharadvaj BK, Sottiurai VS, Mabon RF, Glagov S. Carotid bifurcation atherosclerosis quantitative correlation of plaque localization with flow velocity profiles and wall shear-stress. *Circ Res.* 1983;53:502–514.
4. Pournaras CJ, Rungger-Brandle E, Riva CE, Hardarson H, Stefansson E. Regulation of retinal blood flow in health and disease. *Prog Retin Eye Res.* 2008;27:284–330.
5. Grunwald JE, DuPont J, Riva CE. Retinal haemodynamics in patients with early diabetes mellitus. *Br J Ophthalmol.* 1996;80:327–331.
6. Candido R, Allen TJ. Haemodynamics in microvascular complications in type 1 diabetes. *Diabetes-Metab Res.* 2002;18:286–304.
7. Konno S, Feke GT, Yoshida A, Fujio N, Goger DG, Buzney SM. Retinal blood flow changes in type I diabetes: a long-term follow-up study. *Invest Ophthalmol Vis Sci.* 1996;37:1140–1148.
8. Patel V, Rassam S, Newsom R, Wiek J, Kohner E. Retinal blood flow in diabetic retinopathy. *BMJ.* 1992;305:678–683.
9. Emre M, Orgul S, Gugleta K, Flammer J. Ocular blood flow alteration in glaucoma is related to systemic vascular dysregulation. *Br J Ophthalmol.* 2004;88:662–666.
10. Feke GT, Pasquale LR. Retinal blood flow response to posture change in glaucoma patients compared with healthy subjects. *Ophthalmology.* 2008;115:246–252.
11. Fuchsjager-Mayrl G, Wally B, Georgopoulos M, et al. Ocular blood flow and systemic blood pressure in patients with primary open-angle glaucoma and ocular hypertension. *Invest Ophthalmol Vis Sci.* 2004;45:834–839.
12. Park JS, Choi CK, Kihm KD. Optically sliced micro-PIV using confocal laser scanning microscopy (CLSM). *Exp Fluids.* 2004;37:105–119.
13. Sugii Y, Okuda R, Okamoto K, Madarame H. Velocity measurement of both red blood cells and plasma of in vitro blood flow using high-speed micro PIV technique. *Meas Sci Technol.* 2005;16:1126–1130.
14. Nakano A, Sugii Y, Minamiyama M, Niimi H. Measurement of red cell velocity in microvessels using particle image velocimetry (PIV). *Clin Hemorheol Microcirc.* 2003;29:445–455.
15. Tangelder GJ, Slaaf DW, Muijtjens AMM, Arts T, Egbrink M, Reneman RS. Velocity profiles of blood-platelets and red-blood-cells flowing in arterioles of the rabbit mesentery. *Circ Res.* 1986;59:505–514.
16. Sugii Y, Nishio S, Okamoto K. In vivo PIV measurement of red blood cell velocity field in microvessels considering mesentery motion. *Physiol Measure.* 2002;23:403–416.
17. Logean E, Schmetterer L, Riva CE. Velocity profile of red blood cells in human retinal vessels using confocal scanning laser Doppler velocimetry. *Laser Phys.* 2003;13:45–51.
18. Bishop JJ, Nance PR, Popel AS, Intaglietta M, Johnson PC. Effect of erythrocyte aggregation on velocity profiles in venules. *Am J Physiol Heart Circ Physiol.* 2001;280:H222–H236.
19. Leitgeb R, Schmetterer L, Drexler W, Fercher A, Zawadzki R, Bajraszewski T. Real-time assessment of retinal blood flow with ultrafast acquisition by color Doppler Fourier domain optical coherence tomography. *Opt Express.* 2003;11:3116–3121.
20. Tao YK, Kennedy KM, Izatt JA. Velocity-resolved 3D retinal microvessel imaging using single-pass flow imaging spectral domain optical coherence tomography. *Opt Express.* 2009;17:4177–4188.
21. Song H, Zhao Y, Qi X, Chui YT, Burns SA. Stokes vector analysis of adaptive optics images of the retina. *Opt Lett.* 2008;33:137–139.
22. Burns SA, Tumbar R, Elsner AE, Ferguson D, Hammer DX. Large-field-of-view, modular, stabilized, adaptive-optics-based scanning laser ophthalmoscope. *J Opt Soc Am A.* 2007;24:1313–1326.
23. Chui TYP, Song H, Burns SA. Individual variations in human cone photoreceptor packing density: variations with refractive error. *Invest Ophthalmol Vis Sci.* 2008;49:4679–4687.
24. Roorda A, Romero-Borja F, Donnelly WJ III, Queener H. Adaptive optics scanning laser ophthalmoscopy. *Opt Express.* 2002;10:405.
25. Song H, Qi X, Zou W, Zhong Z, Burns SA. Dual electro-optical modulator polarimeter based on adaptive optics scanning laser ophthalmoscope. *Opt Express.* 2010;18:21892–21904.
26. Ferguson RD, Zhong Z, Hammer DX, et al. Adaptive optics scanning laser ophthalmoscope with integrated wide-field retinal imaging and tracking. *J Opt Soc Am A.* 2010;27:A265–A277.
27. Zou W, Qi X, Burns SA. Wavefront-aberration sorting and correction for a dual-deformable-mirror adaptive-optics system. *Opt Lett.* 2008;33:2602–2604.
28. Hammer DX. Compact scanning laser ophthalmoscope with high-speed retinal tracker. *Appl Opt.* 2003;42:4621–4632.
29. Zhong Z, Petrig BL, Qi X, Burns SA. In vivo measurement of erythrocyte velocity and retinal blood flow using adaptive optics scanning laser ophthalmoscopy. *Opt Express.* 2008;16:12746–12756.
30. Jay AWL. Geometry of human erythrocyte: 1. effect of albumin on cell geometry. *Biophys J.* 1975;15:205–222.
31. Korin N, Bransky A, Dinnar U. Theoretical model and experimental study of red blood cell (RBC) deformation in microchannels. *J Biomech.* 2007;40:2088–2095.
32. Jeong JH, Sugii Y, Minamiyama M, Okamoto K. Measurement of RBC deformation and velocity in capillaries in vivo. *Microvasc Res.* 2006;71:212–217.
33. Venkateswaran K, Roorda A, Romero-Borja F. Theoretical modeling and evaluation of the axial resolution of the adaptive optics scanning laser ophthalmoscope. *J Biomed Opt.* 2004;9:132–138.
34. Secomb TW. Mechanics of blood flow in the microcirculation. *Symp Soc Exp Biol.* 1995;49:305–321.
35. Werkmeister RM, Dragostinoff N, Pircher M, et al. Bidirectional Doppler Fourier-domain optical coherence tomography for measurement of absolute flow velocities in human retinal vessels. *Opt Lett.* 2008;33:2967–2969.
36. Yen RT, Fung YC. Effect of velocity distribution on red-cell distribution in capillary blood-vessels. *Am J Physiol.* 1978;235:H251–H257.
37. Caro CG, Pedley TJ, Schroter RC, Seed WA. *The Mechanics of the Circulation.* Oxford, UK: Oxford University Press; 1978.
38. Tangelder GJ, Slaaf DW, Arts T, Reneman RS. Wall shear rate in arterioles in vivo: least estimates from platelet velocity profiles. *Am J Physiol.* 1988;254:H1059–H1064.
39. Gaehtgens P, Meiselman HJ, Wayland H. Velocity profiles of human blood at normal and reduced hematocrit in glass tubes up to 130 micra diameter. *Microvasc Res.* 1970;2:13–23.
40. Baker M, Wayland H. On-line volume flow-rate and velocity profile measurement for blood in microvessels. *Microvasc Res.* 1974;7:131–143.
41. Kagemann L, Harris A, Chung HS, Evans D, Buck S, Martin B. Heidelberg retinal flowmetry: factors affecting blood flow measurement. *Br J Ophthalmol.* 1998;82:131–136.
42. Shimizu K, Ujie K. *Structure of Ocular Vessels.* New York: Igaku-Schoin Medical Publishers; 1978.